

# PCCP

Accepted Manuscript



This is an *Accepted Manuscript*, which has been through the Royal Society of Chemistry peer review process and has been accepted for publication.

*Accepted Manuscripts* are published online shortly after acceptance, before technical editing, formatting and proof reading. Using this free service, authors can make their results available to the community, in citable form, before we publish the edited article. We will replace this *Accepted Manuscript* with the edited and formatted *Advance Article* as soon as it is available.

You can find more information about *Accepted Manuscripts* in the [Information for Authors](#).

Please note that technical editing may introduce minor changes to the text and/or graphics, which may alter content. The journal's standard [Terms & Conditions](#) and the [Ethical guidelines](#) still apply. In no event shall the Royal Society of Chemistry be held responsible for any errors or omissions in this *Accepted Manuscript* or any consequences arising from the use of any information it contains.



Journal Name

ARTICLE

## The Role of the Local Chemical Environment of Ag on the Resistive Switching Mechanism of Conductive Bridging Random Access Memories

Received 00th January 20xx,  
Accepted 00th January 20xx

DOI: 10.1039/x0xx00000x

www.rsc.org/

E. Souchier,<sup>a</sup> F. D'Acapito,<sup>b</sup> P. Noé,<sup>a</sup> P. Blaise,<sup>a</sup> M. Bernard<sup>a</sup> and V. Jousseume<sup>a,\*</sup>

Conductive Bridging Random Access Memories (CBRAM) are one of the most promising emerging technologies for next generation of non-volatile memory. However, the lack of understanding of the switching mechanism at a nanoscale level prevents a successful transfer to the industry. In this paper, Ag/GeS<sub>x</sub>/W CBRAM devices are analyzed by depth selective X-ray Absorption Spectroscopy before and after switching. The study of the local environment around Ag atoms in such devices reveals that Ag is in two very distinct environments with short Ag-S, due to Ag dissolved in the GeS<sub>x</sub> matrix, and longer Ag-Ag bonds related to an Ag metallic phase. These experiments allow concluding that the switching process involves formation of metallic Ag nano-filaments initiated at the Ag electrode. All these experimental features are well supported by *ab initio* molecular dynamics simulations showing that Ag favorably bonds to S atoms and permit proposing a model at the microscopic level in order to explain the instability of the conductive state in these Ag-GeS<sub>x</sub> CBRAM devices. Finally, the principle of the nondestructive method described here can be extended to other types of resistive memory concepts.

### Introduction

Conductive Bridging Random Access Memories (CBRAM), also called electrochemical metallization cells (ECM) or programmable metallization cells (PMC), are considered to be one of the most promising emerging technologies for next generation of non-volatile memory. These resistive memories, which utilize the reversible switching of a dielectric between two distinct conductive states as mean of logical data storage, are based on the electrochemical growth or dissolution of a conductive nano-filament from metal ions in a solid electrolyte.<sup>1-7</sup> The CBRAM cell is composed of a solid ion-conductor electrolyte thin film (GeS<sub>x</sub>, GeSe<sub>x</sub>, Ag<sub>2</sub>S or oxides) sandwiched between an electrochemically active metal electrode (Ag, Cu, Ni) and an electrochemically inert counter electrode (Pt, Ir, W, Au).<sup>1-8</sup>

This technology is particularly attractive due to the small applied voltage and energy needed for the reversible resistive switching mechanism between the high and low resistance states, the fast programming times, the large non-volatile resistance contrast between the two states ( $R_{ON}/R_{OFF}$  ratio of more than five orders of magnitude) and its expected high scalability.<sup>3-4</sup>

One of the most promising CBRAM consists in an Ag-GeS<sub>x</sub> glass sandwiched between an Ag electrochemically active anode and an inert cathode (Pt or W).<sup>4, 9</sup> The 0 and 1 levels are associated to the resistivity difference between two conductive states due to the diffusion of Ag<sup>+</sup> ions in the chalcogenide glass but the exact switching mechanism remains not fully understood. These glasses are good solid electrolytes with a high Ag ionic conduction at room temperature.<sup>10</sup> It is expected that, under the influence of an electric field, Ag ions are produced at the anode and migrate in the electrolyte to form a conducting path.<sup>3</sup> This process is reversible by applying a bias with opposite polarity. This resistive switching of the material caused by the formation and removal of the conductive pathway can be used for information storage. Although the physical properties of bulk Ag-Ge-S glasses have been well characterized for different glassy systems, these characterizations on thin films (<50 nm thick) are relatively scarce and the fundamental mechanisms of the ionic transport process are not yet fully understood from a microscopic point of view. This is partly due to a lack of structural information particularly in the medium-range order. The structure of amorphous GeS<sub>x</sub> is often depicted as a polymer-like structure containing Ge(S<sub>1/2</sub>)<sub>4</sub> tetrahedron.<sup>11</sup> The tetrahedral units decrease with the increasing Ge composition and, in Ge rich samples, the presence of ethane-like units with Ge-Ge bonds and Ge-S chains is reported. The addition of silver in the chalcogenide causes serious changes in the molecular structure of the material. For instance, Mitkova *et al.* suggested that above a threshold concentration of approximately 2 at% Ag in Ag-Ge-S, a phase separation occurs,

<sup>a</sup> Univ. Grenoble Alpes, F-38000 Grenoble, France,

CEA, LETI, MINATEC Campus, F-38054 Grenoble, France.

<sup>b</sup> CNR-IOM-OGG c/o ESRF, 71, rue des Martyrs, F-38043 Grenoble Cedex 9, France.

† Present address: Dolphin Integration / IBM, souchier@fr.ibm.com Footnotes

\* Corresponding Author: vincent.jousseume@cea.fr

leading to crystalline chalcogenide (e.g.,  $\text{Ag}_2\text{S}$ ) nanoparticles dispersed in the amorphous matrix of the residual material. The  $\text{Ag}_2\text{S}$  nanoparticles showed diameters in the range from 5 to 12 nm.<sup>12,13</sup> However, this phase separation is dependent of the chalcogenide composition, Ge rich samples being more homogeneous and requiring higher annealing temperature (>300°C) to crystallize.<sup>14</sup>

On bulk glasses of  $(1-y)\text{GeS}_2 + y\text{Ag}_2\text{S}$  ( $0.1 < y < 0.5$ ), Ge K-edge Extended X-Ray Absorption Fine Structure (EXAFS) studies have shown that the  $\text{Ag}_2\text{S}$  addition induces a simultaneous depolymerization of edge and corner sharing tetrahedra, which compose the  $\text{GeS}_2$  structure, leading to an increase of short-range order structural distortion.<sup>15</sup> Ag K-edge EXAFS has shown that, for  $\text{Ag}_2\text{S}$ -enriched glassy compositions ( $y > 0.3$ ), the silver environment is close to that in the  $\alpha\text{-Ag}_8\text{GeS}_6$  crystalline phase while for low  $\text{Ag}_2\text{S}$  contents ( $y < 0.3$ ), the silver environment in the glasses is rather similar to that found in  $\alpha\text{-Ag}_2\text{S}$ .<sup>16</sup> Recently, a study on the analysis of the chemical environment of the Ge, S and Ag atoms in Ag-doped  $\text{GeS}_x$  ( $1.6 < x < 2.2$ ) thin films by XANES spectroscopy (X-ray Absorption Near Edge Structure) surprisingly reported that no metallic  $\text{Ag}^0$  is present in such films and that the Ag ions (average oxidation number founded  $\sim 0.3$ ) are preferentially bonded to the Ge atoms with the electronic charges from Ag which preferably transfer to the Ge 4s orbital states.<sup>17,18</sup> But all these results have been obtained in thin films without application of an electrical switching to the material. However, the optimization of these devices needs a better understanding of the Ag environment and on the impact of the switching mechanism on this environment. For this reason, structural studies of Ag-doped germanium chalcogenide glasses should be undertaken in order to establish correlations between the  $\text{Ag}^+$  ionic conduction and the microscopic structure.

In this paper, we report for the first time the characterization of CBRAM devices by depth selective X-ray Absorption Spectroscopy before and after cycles of SET and RESET. These experiments allow answering to several questions related to the  $\text{Ag}^+$  diffusion phenomena in  $\text{Ag-GeS}_x$  glasses and to the structure of this solid electrolyte used in CBRAM devices.

## Experimental

### Materials

The test devices consisted in a 25 nm thick W bottom electrode layer deposited by DC sputtering on a 200 mm Si (100) substrate. Then, a  $\text{GeS}_x$  chalcogenide electrolyte (50 nm thick) was deposited by magnetron sputtering from a pure  $\text{GeS}_2$  target (from Heraeus) under an Ar gas flow on a Clusterline 200 tool (from Oerlikon). The Ag top electrode (20 nm thick) was deposited by DC sputtering in the same cluster tool (without any air break). This Ag layer was deposited through a polymer mask in order to define the device area ( $2 \times 80 \text{ mm}^2$ ). These large devices area were designed in order to perform the XAS measurements in grazing incidence mode and to increase the fraction of material to be analyzed (Figure

1). Finally, after electrical switching but before probing the local order around  $\text{Ag}^+$  ions involved in the SET and the RESET by XAS analysis, the top Ag anode of the CBRAM was completely removed by Ion Beam Etching. A slight over-etching was performed (2-3 nm) in order to be sure to have reached the  $\text{GeS}_x$  layer. Thus, this permits to study only the local order of the silver ions within the chalcogenide glass.

### Electrical characterization

The CBRAM devices to be analyzed by XAS were electrically tested prior to the experiment in order to simulate a CBRAM device in its different states (electrically switched or not). Figure 2 illustrates typical  $I(V)$  curves obtained. The reversible switching from the high to the low resistive state (SET and RESET respectively) was observed despite the somehow very large area of the Ag upper electrode. During the SET, the serial resistance due to the electrical test configuration (large device, bottom electrical contact taken on the 200 mm W electrode far from the device) acted as the current compliance. Depending on the polarization applied between the Ag upper and W lower electrodes, the devices exhibit threshold voltages as low as +0.25 and -1.3 V in order to SET or RESET the memory respectively. The devices showed good cyclability (at least up to 100 cycles). Switched samples analyzed by XAS were cycled 10 time and left in the ON state.

### XAS measurements

Extended X-ray Absorption Fine Structure (EXAFS) measurements have been carried out at the GILDA-CRG beamline of ESRF<sup>19</sup> on an experimental station dedicated to total reflection XAS measurements ("RefLEXAFS").<sup>20</sup> The monochromator was equipped with a pair of Si(311) crystals and was run in dynamically focusing mode. Harmonic rejection was achieved by using a pair of Pt coated mirrors with a cutoff energy of 30 keV. The beam dimensions on the sample position were about 50  $\mu\text{m}$  (vertical) \* 2 mm (horizontal), the vertical dimension being achieved with a slit over a focused beam. The sample was mounted on a stage permitting a precise alignment in total reflection conditions; the intensities of the incoming and reflected beams were measured by an Ion chamber filled with Ar gas. The fluorescence from the sample was collected by using a 12 elements high purity Ge detector with an energy resolution of about 400 eV in the energy region of interest (the Ag-K emission line at 22100 eV). Each sample was aligned on the beam and successively RefLEXAFS spectra at 3 different angles were acquired, collecting both the reflected beam and the fluorescence from the layer. A preliminary calibration of the ion chambers response in the whole energy range covered by the EXAFS spectra permitted an absolute calibration of the reflectivity. Note that in all cases the beam footprint was shorter than the samples in order to obtain absolute values for reflectivity.

## Results

The local order of the  $\text{Ag}^+$  ions involved in the resistive switching of CBRAM was studied on large test devices prepared by magnetron sputtering deposition on 200 mm Si substrates. As detailed in the experimental section, large devices were designed in order to carry out the XAS measurements in grazing incidence mode with the aim of realizing depth-selective measurements and to increase the fraction of material to be analyzed. Before probing the local order around  $\text{Ag}^+$  ions involved in the SET and the RESET by XAS analysis at the Ag-K edge, the top Ag anode of the CBRAM devices was removed by Ion Beam Etching. Thus this allows the study of the local order of the silver ions only within the chalcogenide glass.

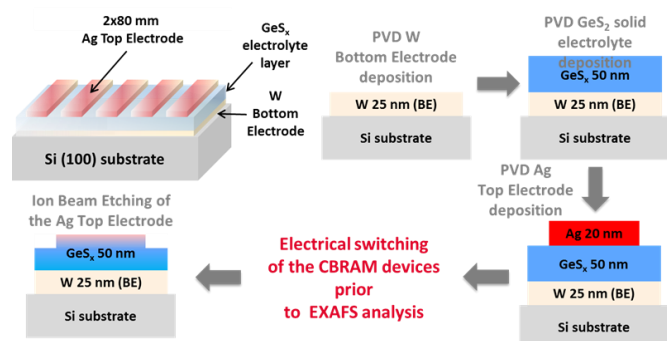


**Figure 1.** Schematic representation of the CBRAM devices and their elaboration process in order to be analyzed by XAS spectroscopy after different SET/RESET operations. The top Ag electrode was removed by Ion Beam Etching prior to the XAS experiment.

The composition of the  $\text{GeS}_x$  chalcogenide thin films used in these CBRAM was measured by Rutherford Back Scattering (RBS) and Particle Induced X-ray Emission (PIXE). The chalcogenide composition is similar before and after electrical switching cycles. As a result, an S/Ge ratio of  $1.44 \pm 0.25$  with an Ag concentration of  $8 \pm 1$  at% were obtained in both configurations (before or after electrical switching). We can notice that the presence of Ag atoms in the  $\text{GeS}_x$  matrix is generally observed in such structures at room temperature without any treatment.<sup>17</sup> This absence of change in the composition before and after switching can indicate that only a very small material change is involved in the switching mechanism or that the change is not in the area probed by RBS analysis.

The CBRAM devices to be analyzed by XAS were electrically tested prior to the experiment in order to simulate a CBRAM device in its different states (electrically switched or not). Figure 2 illustrates typical  $I(V)$  curves obtained. The reversible switching from the high to the low resistive state was observed despite the very large area of the Ag upper electrode. Depending on the polarization applied between the Ag upper and W lower electrodes, the device exhibits threshold voltages as low as +0.25 and -1.3 V in order to SET or RESET the memory respectively. The devices showed good cyclability (at least up to 100 cycles).

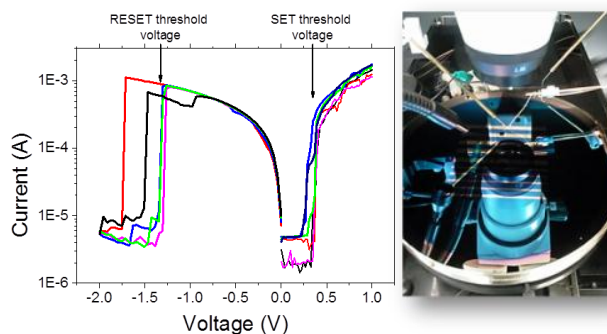


**Figure 2.** (Left) Typical  $I(V)$  curves of a CBRAM device during cycles of SET and RESET between the low and high resistive states. 4 cycles are reported on this example. (Right) Picture of the CBRAM devices during an electrical test.

Switched samples analyzed by XAS were cycled 10 times and left in the ON state. Extended X-ray Absorption Fine Structure measurements have been carried out at the GILDA-CRG beamline of ESRF. RefLEXAFS spectra at 3 different angles were acquired, collecting both the reflected beam and the fluorescence from the layer (Figure 3).

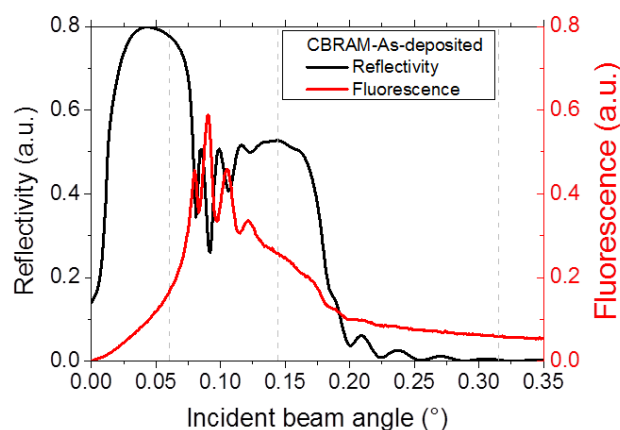


**Figure 3.** Reflectivity and fluorescence curves collected on non-switched as-deposited CBRAM sample at 25600 eV. The dashed lines indicate the collection angles for RefLEXAFS data chosen to enhance the sensitivity to different zones of the sample: 0.06 degree for the surface (4 nm),  $\sim 0.15$  degree for the chalcogenide layer and 0.32 degree for the deep part of the sample.

The 3 angles define different probing zones of the sample: the surface (collected at 0.06° i.e. with the beam reflected at the sample surface). The extinction length of the probe beam is estimated to about 4 nm, the layer (collected at  $\sim 0.15^\circ$  with the beam reflected at the chalcogenide-W interface so shining the whole Ag- $\text{GeS}_x$  layer) and the depth collected at 0.32° with the probe beam penetrating also into the W layer.

A preliminary calibration of the ion chambers response in the whole energy range covered by the EXAFS spectra permitted an absolute calibration of the reflectivity. Note that in all cases the beam footprint was shorter than the samples in order to

obtain absolute values for reflectivity. The data in fluorescence mode were analyzed via standard methods with the ATHENA and ARTEMIS codes respectively for data extraction and quantitative fit.<sup>21</sup> RefLEXAFS data were analyzed by using the CARD code.<sup>22,23</sup> The RefLEXAFS data are guaranteed to be relative to the surface of the sample (the fluorescence data could in principle be contaminated by bulk contributions in case of high roughness) and are presented to validate the fluorescence data in total reflection conditions. In all cases the theoretical EXAFS paths were generated with the Feff8 code.<sup>23</sup> Clusters from metallic Ag and Ag<sub>2</sub>S were used as starting structures and the structural model used for the data fit consisted in a balanced mix of these two phases. Metallic Ag was taken into account with 4 coordination shells (totally 5 scattering paths) whereas for the sulphide, only the first shell was considered. Free fit parameters were the relative amount metal/sulphide, the Ag-S bond length and Debye-Waller factor (DWF), and the overall metallic Ag lattice parameter. For the dynamic part of the metal, the first Ag-Ag shell was modeled using DWF while a Debye model (with a single free Debye temperature) was used for the other shells in order to reduce the number of free parameters.

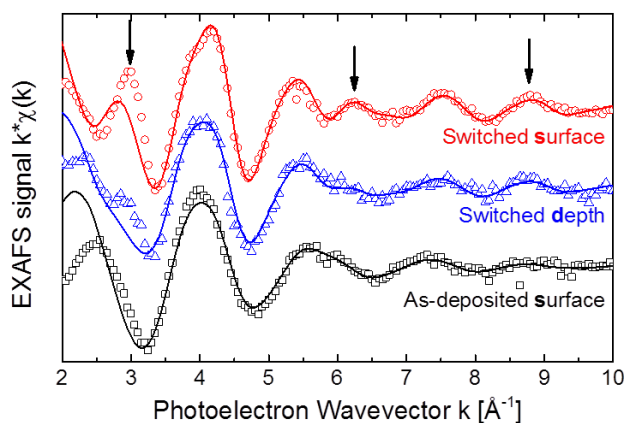


**Figure 4.** EXAFS spectra of 3 prototypical samples (switched CBRAM sample using surface and depth collection mode and a non-switched as-deposited CBRAM sample on the surface) with the best fit curves (continuous lines). The vertical lines mark the features that grow for increasing Ag-metal content.

The coordination numbers were fixed to the crystallographic values for the metal and to 2.3 S for the sulphide phase following a fit on a pure sulphide phase sample. In all the studied cases, the fits of the reflectivity curves yielded similar results (errors are about 10 % of the value) with a 50 nm Ag-GeS<sub>x</sub> layer with a roughness of 1.5 – 2.0 nm and a W layer of 30 nm. The EXAFS data of 3 prototypical samples are shown in figure 4 whereas the related Fourier Transforms (FT) are shown in figure 5. The FT exhibit two main peaks that have been identified as due to Ag-S and Ag-Ag correlations. The principal difference is the intensity of the second peak in the FT (figure 5) and correspondingly, additional oscillations are visible in the EXAFS spectra (figure 4). An example of results of the quantitative EXAFS analysis is shown in Table 1. An Ag-S

shell at ~2.5 Å is revealed whereas an Ag-Ag correlation at ~2.88 Å. This latter value is typical of Ag-Ag bond in the metallic fraction and attempts to reproduce this contribution with an Ag-Ge contribution yielded to unphysical results.

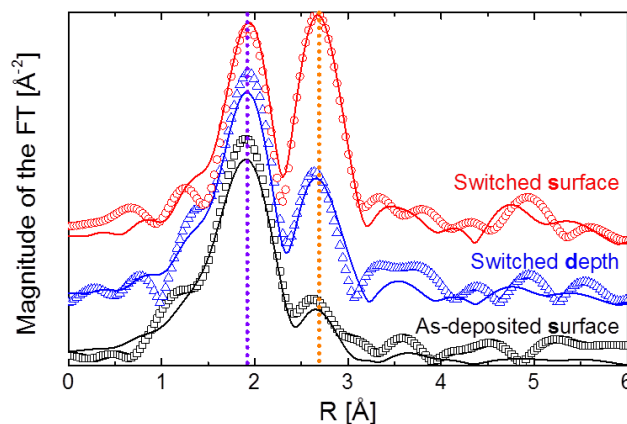


**Figure 5.** Fourier Transforms of the spectra presented in Fig. 4 with the related best fit curves (continuous lines). The transforms were carried out in the interval  $k = [2.6-9.5] \text{ \AA}^{-1}$  and the fit was carried out in R space on  $k^2$  weighted spectra in the interval  $R = [1.5-5.8] \text{ \AA}$ . The vertical lines mark the position of the Ag-S (violet) and Ag-Ag (orange) bonds, the latter exhibiting a reduced height for decreasing metal content.

**Table 1.** Results of the quantitative analysis of the EXAFS data on the switched CBRAM sample collected in surface, layer and depth modes. The suffixes fluo and refl denote respectively data in fluorescence or reflectivity modes.

Sample	Met. Frac. (%)	$R_{\text{Ag-S}}$ (Å)	$\sigma^2_{\text{Ag-S}}$ (Å <sup>2</sup> )	$R_{\text{Ag-Ag}}$ (Å)	$\sigma^2_{\text{Ag-Ag}}$ (Å <sup>2</sup> )
Surf fluo	30 (4)	2.48 (2)	0.016 (2)	2.86 (3)	0.013 (2)
Surf refl	30 (10)	2.48 (2)	0.012 (4)	2.89 (3)	0.011 (4)
Layer fluo	15 (2)	2.50 (2)	0.016 (2)	2.85 (2)	0.012 (3)
Depth fluo	14 (2)	2.49 (2)	0.016 (2)	2.86 (3)	0.011 (2)

The metallic fraction was derived from the reduction of the observed Ag-Ag coordination numbers respect to the crystallographic value (12) and supposing that the reduction is exclusively due to the presence of the sulphide phase. A general behavior, confirmed also by the other samples, is that the metal content is higher for spectra collected at the surface in comparison to spectra collected in the depth and that the switched samples contain the highest amount of metal. Figure 6 presents the data for the metallic fraction parameter for CBRAM samples in the switched and non-switched forms.



## Journal Name

## ARTICLE

**Table 2.** Mean chemical bond lengths evaluated from *ab initio* calculations in DFT/LSDA, plus the mean Bader charge performed for Silver cation. The values indicated in brackets are the corresponding standard deviations of the calculated values.

Distance in Å (std. dev.)	fcc-Ag	m-Ag <sub>2</sub> S	I-GeS <sub>2</sub>	α-Ag <sub>8</sub> GeS <sub>6</sub>	fcc-Ag + GeS <sub>2</sub>	fcc-Ag + GeS <sub>2</sub> + annealing	Experimental results obtained in this study
Ag-Ag	2.89 (0.00)	3.10 (0.10)		3.04 (0.12)	2.89 (0.13)	2.95 (0.18)	2.86 (0.03)
Ag-S		2.61 (0.11)		2.59 (0.08)	2.62 (0.13)	2.61 (0.13)	2.49 (0.03)
Ag-Ge					2.73 (0.08)	2.71 (0.16)	
S-Ge			2.25 (0.01)	2.24 (0.01)	2.27 (0.06)	2.31 (0.10)	
Ge-Ge						2.47 (0.00)*	
Bader charge for Silver	0.00 (0.00)	0.29 (0.01)		0.30 (0.02)	0.10 (0.05)	0.24 (0.08)	

\*only one Ge-Ge bond has appeared after thermal annealing

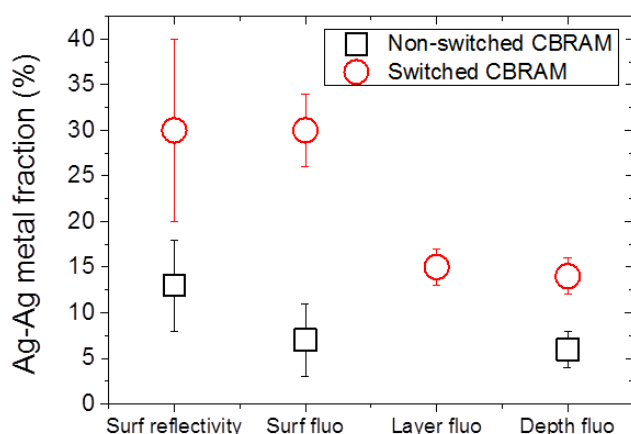


**Figure 6.** Metallic fraction values detected at the different sampling regions for the non-switched and switched samples.

*Ab initio* simulations were performed in order to support the analysis of our experimental data. First of all, several representative systems were calculated: pure fcc-silver, the low temperature monoclinic form of Ag<sub>2</sub>S,<sup>24</sup> a known orthorhombic I-GeS<sub>2</sub>,<sup>25</sup> and the low temperature α-Ag<sub>8</sub>GeS<sub>6</sub>.<sup>26</sup> Calculations were performed in DFT/LSDA<sup>27</sup> (Density Functional Theory in Local Spin Density Approximation) using linear combinations of numerical atomic orbitals with the Siesta code.<sup>28</sup> A DZP (double-zeta basis plus polarization orbitals) scheme with a 50 meV shift was used, using Troullier-Martins pseudopotentials,<sup>29</sup> including a relativistic plus a semi-core correction for silver. Forces and stress were minimized below 0.02 eV/Å and 200 MPa respectively for each structure minimization calculation.

In order to study silver alloying with GeS<sub>2</sub>, two monolayers of fcc-Ag sandwiched between 2 nm of I-GeS<sub>2</sub> was first relaxed

for a system made of 280 atoms (64.Ag + 72.GeS<sub>2</sub>). Then, the effect of a thermal annealing was simulated by *ab initio* molecular dynamics (AIMD), applying a mean temperature of 1000 Kelvin (below the GeS<sub>2</sub> melting point) for 18 ps, followed by 15 ps of cooling down to 300 K plus a last minimization step. Extracted structural data from our calculations are shown in table 2. DFT/LSDA shows a global agreement with available experimental data on pure compound, with an Ag-Ag bond at 2.89 Å in pure silver that increases to 3.03 Å in α-Ag<sub>8</sub>GeS<sub>6</sub> and 3.10 Å in m-Ag<sub>2</sub>S. In comparison the Ge-S bond is almost constant at 2.24 - 2.25 Å as the Ag-S bond at 2.59 - 2.61 Å for pure compounds. For comparison DFT/GGA calculations have been performed for the I-GeS<sub>2</sub> structure giving a Ge-S bond at 2.28 Å. Moreover LSDA shows a volume per unit cell decrease of 2.6% compare to a large volume increase of 15.1% in GGA. This large volume mismatch in GGA has already been reported elsewhere for various forms of GeSe<sub>2</sub><sup>30</sup> and is probably related to van der Waals interaction that would have required a better treatment using a more advanced functional. Nevertheless, in order to perform AIMD at a reasonable computational cost without artificially increasing the stress between Ag and GeS<sub>2</sub> layers the whole study has been performed by keeping LSDA functional.

## Discussion

The Ag-S bond length found by XAS is 2.50 Å, in agreement with what is found in the Ag<sub>2</sub>S Acanthite mineral<sup>21</sup> that present distances in the range 2.5-2.6 Å. The Ag-S coordination number (CN) measured in an unswitched sample presenting no Ag-Ag bonds was found to be 2.50(5). This value is in agreement with the observed bond length as we verified that

Bond Valence Method<sup>22</sup> applied to the  $\text{Ag}^+\text{S}^{2-}$  pair predicts a distance of 2.52 Å for a 3 coordinated metal. Because no further coordination shells were visible in that sample, we deduce that Ag is dissolved in the glassy  $\text{GeS}_x$  matrix, the second Ag-Ge shell being not revealed probably due to structural disorder (as already noticed in Ref. [17] for the Ge-K edge). On the other hand, an Ag-Ag bond is revealed in all the samples that is related to the metallic phase of silver. Indeed the observed distance (2.85-2.90 Å) is in excellent agreement with that of the metallic phase ( $R_{\text{Ag-Ag}} = 2.88$  Å) and not with the  $\text{Ag}_2\text{S}$  phase which exhibits Ag-Ag distances well above 3 Å. The two phases (metal and sulphur bound) are in competition as when the Ag-Ag CN increases the Ag-S CN correspondingly decreases. The amount of metal observed as a function of the switching state or the depth is of particular interest for the comprehension of the working principles of this device. Figure 6 clearly shows that CBRAM samples that never have undergone any switching process presents a lower metal fraction (about 0-15 %) whereas the switched ones have a higher value of metallic Ag. Moreover, the surface data (we recall here that the probed layer in this case is about 4 nm thick) show a higher metal fraction when compared with the data coming from the entire layer. From these considerations, it is possible to conclude that the switching process involves the formation of metallic Ag and that the formation of this phase is initiated at the Ag electrode. This supports the model of filaments or conducting paths consisting in cones with their base on the active electrode. This morphology has been already observed experimentally in  $\text{Ag/a-Si/Pt}$ <sup>31</sup>,  $\text{Ag/SiO}_2/\text{Pt}$ <sup>32</sup> and  $\text{Cu/Al}_2\text{O}_3/\text{TiN}$ <sup>33</sup> structures and is a consequence of the fact that the metal reduction happens more rapidly than the ion migration.

Recently, Cho *et al.* have reported on the charge transfer from Ag to Ge in the  $\text{GeS}_x$  matrix observed using XANES,<sup>17</sup> which seems contradictory to our observation that no Ag-Ge bonds are detectable by EXAFS. In reference [17], the authors have reported that upon doping  $\text{GeS}_x$  by Ag, Ag is indeed ionized ( $\text{Ag}^{\sim 0.3}$ ) and the electronic charges from Ag preferably transfer to the Ge 4s orbital states. By taking simply into account the electronegativity of each Ag, Ge and S element, which are respectively 1.93, 2.01 and 2.58 on Pauling scale,<sup>34</sup> when Ag is incorporated in  $\text{GeS}_x$ , Ge is still positively charged because it remains mainly bonded to S atoms, but a small amount of Ag-Ge bonds can modify the Ge charge and strongly affect the Ge L-edges in XANES. This is not contradictory with our present EXAFS results for which no significant Ag-Ge bonds have been detected in the EXAFS spectra at Ag K-edges due to the possible small amount of Ag-Ge bonds compared to Ag-S and Ag-Ag bonds. Moreover, a shift in the XANES spectra of Ge does not indicate that Ge preferentially bonds to Ag and a slight percentage of Ag-Ge bonds can largely produce a significant shift of Ge edge from a largely positive charge in  $\text{GeS}_x$  to a positive charge weighted by the significant shift due to the presence of Ag-Ge bonds as measured in reference [17]. Finally, our description of the switching mechanisms at the atomic level in Ag- $\text{GeS}_x$  CBRAM allow interpreting also the low data retention reported for this type of devices.<sup>9</sup> Indeed,

assuming that Ag favorably bonds to S atoms, the instability of the ON state can be attributed to Ag sulfidation and hence rupture of the Ag-Ag metallic nano-filaments. In order to confirm this hypothesis and to have a better insight on the physical mechanism governing the data retention at high temperature, AIMD has been performed to study the effect of temperature and time on an Ag-based filament embedded between two  $\text{GeS}_2$  layers (see previous paragraph). The pair correlation functions of the system before and after thermal treatment are both shown in figure 7. The original Ag-Ag peak at 2.8-2.9 Å from the silver layer almost disappears to the benefit of an Ag-S peak at 2.6 Å approximately, which is in agreement with local reordering due to silver alloying with sulfur inside the  $\text{GeS}_2$  matrix.

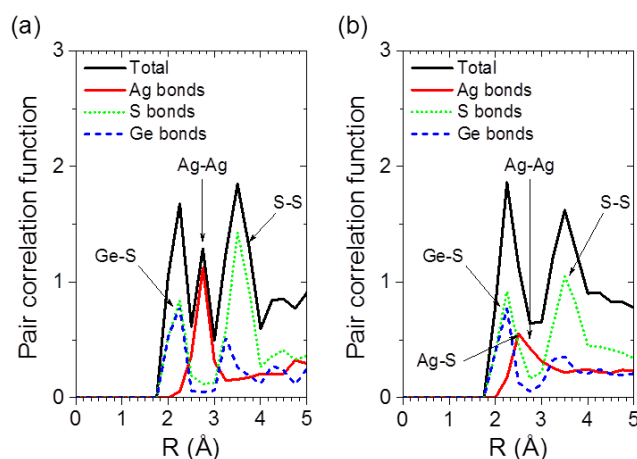


**Figure 7.** Pair correlation function in DFT/LSDA: (a) Silver layer sandwiched by  $\text{GeS}_2$  and (b) Silver sulfidation after simulated thermal annealing at 700°C for ps (1000K).

As shown in figure 8 under thermal annealing Ag atoms more favorably bonds to S atoms and the metallic Ag monolayers are almost completely dissolved in the  $\text{GeS}_2$  matrix by forming various Ag-S and Ag-Ge-S compounds.

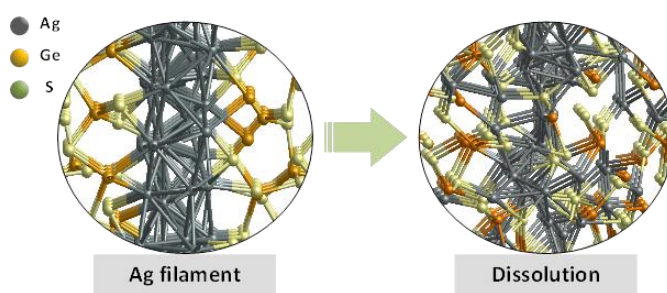


**Figure 8.** Schematic of a silver nano-filament in  $\text{Ag-GeS}_x$  and silver filament dissolution scheme.

We note that raising the temperature at 1000K for ps allows describing the atomistic reorganization of the system that would occur in hours at moderate temperature. This last result is in good agreement with the EXAFS observation showing that the switching process involves the formation of metallic Ag in

the Ag-GeS<sub>x</sub> matrix and that the instability of the ON state (retention) is due to Ag re-sulfidation in the matrix. Moreover, a Bader charge analysis (table 2) shows that this sulfidation process is accompanied by an increase of the silver net positive charge, from +0.10 to +0.24 becoming very close to +0.29 or +0.30 obtained for m-Ag<sub>2</sub>S and α-Ag<sub>8</sub>GeS<sub>6</sub> respectively. As we have previously shown, Sb doping of the GeS<sub>x</sub> matrix can significantly improve the data retention and the stability of the ON state.<sup>35</sup> Indeed, by creating Sb-S compounds, Sb reduces the available S thus limiting the Ag diffusion and metal conduction path dissolution by formation of Ag-S bonds. This type of approach (limitation of filament dissolution due to Ag sulfidation) should be used to improve the data retention of Ag-GeS<sub>x</sub> based CBRAM.

## Conclusion

This work shows the characterization of Ag-GeS<sub>x</sub> CBRAM devices by mean of depth selective X-ray Absorption Spectroscopy before and after cycles of SET and RESET. The study of the local environment around Ag atoms in such devices revealed that Ag is in two very distinct environments with short Ag-S due to Ag dissolved in the GeS<sub>x</sub> matrix and longer Ag-Ag bonds related to an Ag metallic phase. CBRAM samples that never have undergone any switching process are showing a lower metal fraction whereas the switched ones present a higher value. Moreover, RefLEXAFS surface data (the topmost 4 nm) show a higher metal fraction when compared with the data coming from the entire layer. The switching process involves formation of metallic Ag and the formation of this phase is initiated at the Ag electrode. This supports a model for the filaments or conducting nano-filaments consisting in Ag metallic cones with their base on the active electrode as a consequence to the fact that the metal reduction happens more rapidly than the ion migration. All these experimental features are well supported by AIMD simulations showing that Ag favorably bonds to S atoms and allow proposing that the instability of the ON state can be attributed to Ag sulfidation and hence rupture of the Ag-Ag metallic conduction path or filament in the devices. Finally, the principle of the nondestructive method described here can be extended to other types of ECM and will give clues on the understanding of the behavior of resistive RAM.

## Acknowledgements

The authors thank Josie Peyron for support on Ion Beam Etching and François Pierre for support on RBS and PIXE analyses.

## References

- M. Kund, G. Beitel, C.U. Pinnow, T. Rohr, J. Schumann, R. Symanczyk, K.D. Ufert, G. Muller, *Proceeding of the International Electron Devices Meeting 2005*, 773.
- M. Kozicki, M. Park, M. Mitkova, *IEEE Trans. Nanotechnology* 2005, **4**, 331.
- R. Waser, R. Dittman, G. Staikov, K. Szot, *Adv. Mater.* 2009, **21**, 2632-2663.
- C. Gopalan, Y. Ma, T. Gallo, J. Wang, E. Runnion, J. Saenz, F. Koushan, P. Blanchard, S. Hollmer, *Solid State Electron.* 2011, **58**, 54.
- I. Valov, R. Waser, J.R. Jameson, M.N. Kozicki, *Nanotechnology* 2011, **22**, 254003.
- C.-P. Hsiung, H.-W. Liao, J.-Y. Gan, T.-B. Wu, J.-C. Hwang, F. Chen, M.-J. Tsai, *ACS Nano* 2010, **4**, 5414 - 5420.
- Q. Liu, S. Long, H. Lv, W. Wang, J. Niu, Z. Huo, J. Chen, M. Liu *ACS Nano* 2010, **4**, 6162 - 6168.
- Y. Bernard, V.T. Renard, P. Gonon, V. Jousseume *Microelectron. Eng.* 2011, **88**, 814.
- F. Longnos, E. Vianello, C. Cagli, G. Molas, E. Souchier, P. Blaise, C. Carabasse, G. Rodriguez, V. Jousseume, B. De Salvo, F. Dahmani, P. Verrier, D. Bretegnier, J. Liebault, *Solid State Electronics* 2013, **84**, 155-159.
- M. Frumar, T. Wagner, *Current Opinion in Solid State and Materials Science* 2003, **7**, 117.
- Y. Sakaguchi, D.A. Tenne, M. Mitkova, *J. Non-Cryst. Solids* 2009, **335**, 1792-1796.
- M. Mitkova, M.N. Kozicki, H.C. Kim, T.L. Alford, *J. Non-Cryst. Solids* 2006, **352**, 1986- 1990.
- M. Balakrishnan, M. Kozicki, C. Poweleit, S. Bhagat, T. Alford, M. Mitkova, *J. Non-Cryst. Solids* 2007, **353**, 1454.
- R. Bruchhaus, M. Honal, R. Symanczyk, M. Kund, *J. Electrochem. Soc.* 2009, **156**, H729-H733.
- P. Armand, A. Ibanez, H. Dexpert, E. Philippot, *J. Non-Cryst. Solids* 1992, **139**, 137.
- A. Ibanez, P. Armand, H. Dexpert, E. Philippot, *Solid State Ionics* 1993, **59**, 157.
- D.-Y. Cho, I. Valov, J. Van Den Hurk, S. Tappertzhofen, R. Waser, *Adv. Mater.* 2012, **24**, 4552-4556.
- J. Van Den Hurk, A.-C. Dippel, D.-Y. Cho, J. Straquadine, U. Breuer, P. Walter, R. Waiser, I. Valov, *Phys. Chem. Chem. Phys.* 2014, **16**, 18217.
- F. D'Acapito, A. Trapananti, S. Torrenco, S. Mobilio, *Notiziario Neutroni e Luce di Sincrotrone*, 2014, **19**, 1592-7822.
- F. D'Acapito, I. Davoli, P. Ghigna, S. Mobilio, *Journal of Synchrotron Radiation* 2003, **10**, 260-264.
- B. Ravel, M. Newville, *J. Synchrotron Rad.* 2005, **12**, 537-541.
- F. Benzi, I. Davoli, M. Rovezzi, F. d'Acapito, *Review of Scientific Instruments* 2008, **79**, 103902.
- T. Costanzo, F. Benzi, P. Ghigna, S. Pin, G. Spinolo, F. d'Acapito, *J. Synchrotron Rad.* 2014, **21**, 395-400.
- R. Sadanaga, S. Sueno, *Mineral. J. (Japan)* 1967, **5**, 124.
- W. H. Zachariasen, *J. Chem. Phys.* 1936, **4**, 618.
- G. Eulenberger, *Monat. für Chem.* 1977, **108**, 901.
- S. H. Vosko, L. Wilk, M. Nusair, *Can. J. Phys.* 1980, **58**, 1200.
- J.M. Soler, O. Artacho, J.D. Gale, A. Garcia, J. Junquera, P. Ordejon, D. Sanchez-Portal, *J. Phys. Cond. Matter.* 2002, **14**, 2745.
- N. Troullier, J.L. Martins, *Phys. Rev. B* 1991, **43**, 1993.
- M. Fuentes-Cabrera, H. Wang, O.F. Sankey, *J. Phys. Condens. Mater.* 2002, **14**, 9589
- Y. Yang, W. Lu, *Nanoscale* 2013, **5**, 10076.
- Y. Yang, P. Gao, S. Gaba, T. Chang, X. Pan, W. Lu, *Nature Communications* 2012, **3**, 732.
- U. Celano, L. Goux, A. Belmonte, K. Opsomer, A. Flanquet, A. Schulze, C. Detavernier, O. Richard, H. Bender, M. Jurkzac, W. Vandervost, *Nanoletters* 2014, **14**, 2401.
- CRC Handbook of Chemistry and Physics*, W.M. Haynes, 95th edition, 2014.
- E. Vianello, G. Molas, F. Longnos, P. Blaise, E. Souchier, C. Cagli, G. Palma, J. Guy, M. Bernard, M. Reyboz, G. Rodriguez, A. Roule, C. Carabasse, V. Jousseume, S. Maitrejan, G. Reimbold, B. De Salvo, F. Dahmani, P. Verrier, D. Bretegnier,

ARTICLE

Journal Name

J. Liebault, *Proceeding of the International Electron Devices Meeting 2012*, 741.

Physical Chemistry Chemical Physics Accepted Manuscript